The impact of the location of Cu substitutions and electric field on visible light absorption in defective titanium dioxide: *ab initio* calculations

LEI LI*, WENSHI LI, JIAN-FENG YANG, LING-FENG MAO*
Institute of Intelligent Structure and System, School of Electronics & Information Engineering, Soochow University, Suzhou 215006, P.R. China

Metal-dopants have been wildly considered as the effective strategy to improve the visible-light absorption in defective rutile TiO_2. It's necessary to understand the role of metal-substitution in TiO_2 bulk on the visible-light absorption of titanium dioxide. Cu-substitutions have been addressed to illustrate the detailed relationship between their location and visible-light absorption by *ab initio* calculations. The effective of applied electric field on the structure of titanium dioxide has also been studied in detail. The results show that the visible-light absorption of titanium dioxide will be determined by both Cu-substitution and applied electric field.

(Received May 11, 2016; accepted February 12, 2018)

Keywords: Visible-light absorption; Titanium dioxide; Cu-substitutions; *Ab initio* calculations

1. Introduction

In recent years, transparent conductive oxides (TCOs) have attracted great attentions due to their application in the transparent electrical contacts or electrodes in flat panel displays, touch screens, and thin film solar cells [1–3]. Both high electrical conductivity and high visible light transparency determine the performance of transparent conductive oxides. Defective binary oxides, such as SnO_2, ZnO, Nb_2O_5 and TiO_2, have been proposed as transparent conductive oxides. Moreover, these metals, *e.g.*, Ag, Cu, Au, Pt, and Al, are inserted in the TCO/metal/TCO structure acting as the transparent composite electrode [4–6]. In 1972, Honda and Fujishima discovered the electrolysis of water on the TiO_2 electrodes [7]. Several previous studies had reported that the defective TiO_2 with the oxygen vacancies exhibited the n-type semiconductor characteristics. Those defects, such as oxygen vacancies, Ti interstitials and external substitutions, narrow the bandgap of TiO_2 to improve the absorption of visible light [8–14]. Metal-ions substituting for Ti^{4+}-ions, such as Pt and Cr, benefit the production of oxygen vacancies and so improve the visible light absorption [15]. Doping of the transition-metal-ions, such as Fe^{3+} and Cu^{2+}, produces the electrons trapping center to inhibit electrons-holes recombination and also improve the visible light absorption [16–20]. To further clarify the atom-level mechanism of the visible light absorption of TiO_2 based transparent conductive oxides, this work would investigate the impact of the location of Cu substitutions and applied electric fields on optical properties in defective TiO_2 by DFT calculation.

2. Method

One purpose of our work was to illustrate the effect of substitution on the visible light absorption of TiO_2 bulk rather than on its surface, where the vacuum-layer (> 15Å) would be considered over the surface model. The effect of applied electric field on the visible light absorption of TiO_2 bulk mainly focused on [001] direction, which meant that TiO_2 bulk must be thick enough to acquire high computational accuracy. Accordingly, 1×1×6 supercells (a=b=4.594 Å, c=17.754 Å) were constructed based on the primitive cell (a=b=4.594 Å, c=2.959 Å), as shown in Fig. 1(a). The balls in gray, red, dark and pink indicated the Ti-ions, O-ions, oxygen vacancies, and Cu substitutions, respectively. We substituted three oxygen vacancies (marked by the black circles) for three oxygen ions on the same-side or different-sides around the central-Ti-ions (pointed by black-arrows) as shown in the process (1). The detailed values of applied electric fields along Z-direction ([001] direction) in DMol^3 package were (0, 0, 0.0025 *a.u.*) or (0, 0, 0.02 *a.u.*), that corresponded to 1.3 MV/cm or 10.4 MV/cm, respectively. After the structures had been relaxed at 1.3 MV/cm, these structures with three oxygen vacancies were named "*VOSA*" and "*VODF*", respectively. Then, Cu-ions substituted three oxygen vacancies as shown in the process (2). So, the structures with three Cu-substitutions on the same-side or different-sides were named "*CuSA*" or "*CuDF*", respectively. Both two structures above were relaxed by electric fields of 1.3 MV/cm or 10.4 MV/cm along Z-direction.

The DMol^3 package with the spin-polarized method was employed to expand the physical wave functions [21−24]. The geometries relaxation and the electronic properties (density of states and deformation electron density) were processed by PBE (Perdew−Burke−Ernzerhof) formulation in the generalized

gradient approximation [25]. The double-numeric quality basis set (DNP) of 3.5 was used to describe the exchange and correlation effects. High symmetry sampling points in the Brillouin zone were applied in the Monkhorst–Pack schemes with 3×3×1 k-point meshes [26]. A thermal smearing of 0.005 Ha (1 Ha = 27.2114 eV) and a global orbital cut-off of 5.2 Å were set to improve computational efficiency. The minimum tolerances of energy, gradient and displacement convergence for the geometric relaxation and energy calculation were set to 1×10^{-5} Ha, 2×10^{-3} Ha/Å, and 5×10^{-3} Å, respectively. The absorption spectra were calculated by CASTEP package [27] with these sets of ultrasoft-pseudopotentials, the wave basis set with a cutoff energy of 400.0 eV, and the k-points of 3×3×1 meshes. We further employed Virtual Nanolab program to calculate the transmission coefficient with the DFT-PBE functional at 300K [28,29]. The cut-off of the grid mesh was set to 40 Ha The basis sets of double zetas and polarization orbitals (DZP) were performed in the transport simulations.

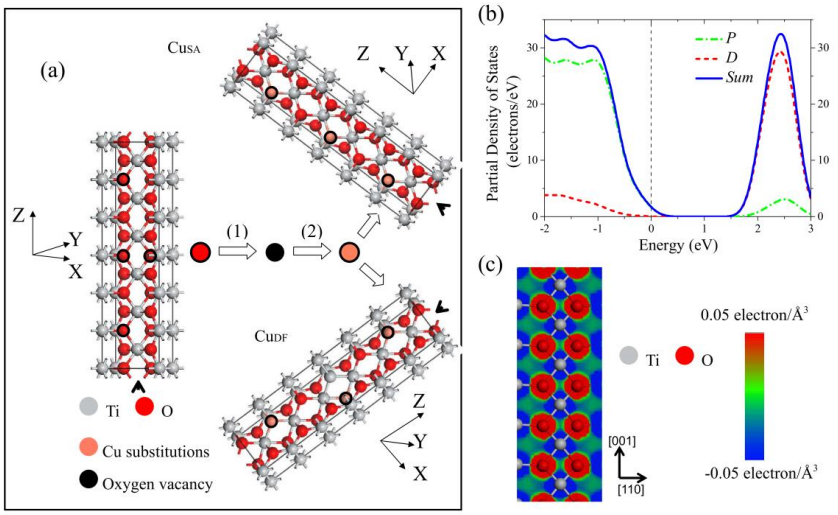

Fig. 1 (a) Structure configuration of the defect-free TiO_2 and the defective TiO_2 with the Cu-substitutions on the same-side (CuSA) and on the different-sides (CuDF) around central-Ti-ions (marked by black-arrows); (b) Density of states and (c) deformation electron density at [110] facet of the defect-free TiO_2.

3. Results and discussions

Fig. 1(b)-1(c) illustrate the partial density of states and the deformation electron density at [110] facet of defect-free TiO_2, respectively. The Ti-ions and O-ions are indicated by the gray and red balls, respectively. The spectrum of deformation electron density is set to the blue-green-red from -0.05 to 0.05 electron/Å^3. The electrons deficiencies are marked in blue, while the electrons enrichment in red. In Fig. 1(b), Fermi level (0 eV) locates above the valence band maximum. The conduction band and the valence band mainly originate from the contribution of Ti-3d and O-2p orbital electrons, respectively. The band gap of perfect TiO_2 (2.04 eV) is far lower than the experimental value of 3.0 eV. It is well recognized that DFT-PBE functional underestimates the bandgap of transition-metal oxides due to well-known self-interaction error. In Fig. 1(c), the electron enrichment in red locates round the O-ions, which means that the O-ions obtain the electrons from the Ti-ions.

Fig. 2 shows the partial density of states in *VOSA* (a) and *VODF* (b) under 1.3 MV/cm, *CuSA* under 1.3 MV/cm (c) and 10.4 MV/cm (d), *CuDF* under 1.3 MV/cm (e) and 10.4 MV/cm (f). The black-dash lines indicate Fermi levels at 0 eV. The green-dash-dot lines, red-dash lines, blue-solid lines represent the p-states, d-states, and sum states, respectively. The black-dot lines indicate the contribution of Cu-3d states. In Figs. 2(a)-2(b), Fermi levels locate below the conduction band minimum. In Figs. 2(c)-2(f), due to the occurrence of the Cu-substitutions, one peak (peak 1) locates below the conduction band minimum and another one (peak 2) locates above the valence band maximum. The former mainly originates from the Ti-3d orbital electrons, while the latter from the Cu-3d orbital electrons. The Cu-substitutions loss electrons, while the lattice Ti^{4+} ions gain electrons to be reduced to Ti^{3+} ions. It implies more excited states that can improve the absorption of visible light to enhance the photocatalytic activities. The peak 2 in Fig. 2(c) locates at (-2.92 19.90), while in Fig. 2(d) at (-2.94 19.71); by contrast, the peak 2 in Fig. 2(e) locates at (-2.83 21.90), while in Fig. 2(f) at (-2.83 21.72). It means that the lower defect energy level in *CuSA* is lower than that in *CuDF*, which could easily excite the holes. The larger density of states in the defect energy levels below the conduction band minimum in Figs. 2(c)-2(d) can excite more delocalized electrons. Thus, the electrons-holes recombination would be more severe in *CuSA* than that in *CuDF*. It leads to that a higher absorption occurs in *CuDF* as shown in Fig. 4. Furthermore, the higher states of peak 2 in Fig. 2(c) or Fig. 2(e) also show more excited holes bring more recombination of electrons-holes. So, the larger electric field lowers down the recombination.

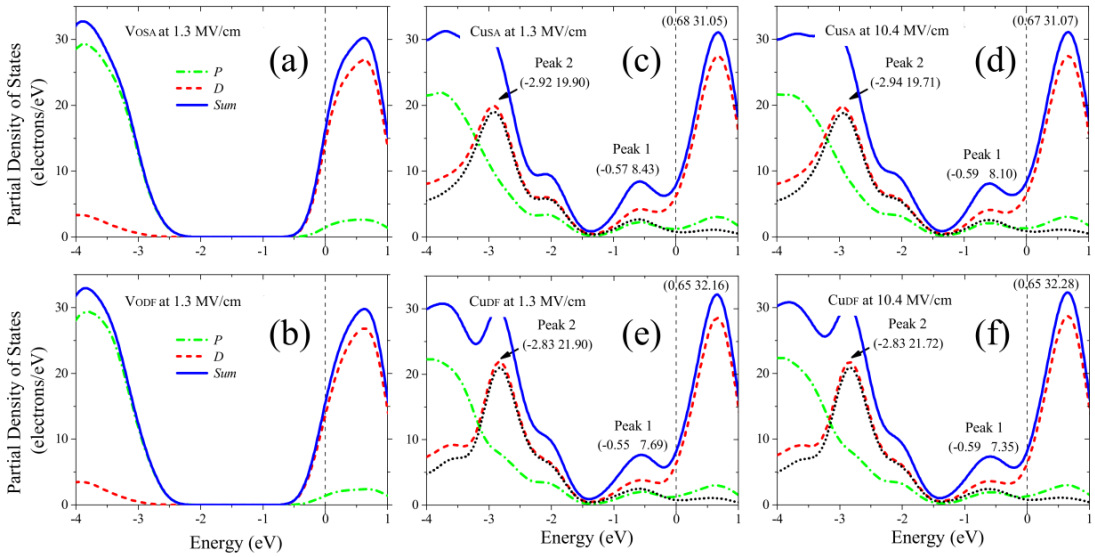

Fig. 2. Partial density of states in VOSA (a) and VODF (b) under 1.3 MV/cm, CuSA under 1.3 MV/cm (c) and 10.4 MV/cm (d), CuDF under 1.3 MV/cm (e) and 10.4 MV/cm (f).

Fig. 3 depicts the partial sectional view at [110] facet and the corresponding deformation electron density of *VOSA* under 1.3 MV/cm (a, b), *CuSA* under 1.3 MV/cm (c, d) and 10.4 MV/cm (e, f), *VODF* under 1.3 MV/cm (g, h), *CuDF* under 1.3 MV/cm (i, j) and 10.4 MV/cm (k, l). The deformation electron density equals to the total density with the density of the isolated atoms subtracted. We set the spectrum of deformation electron density to the blue-green-red, which is from -0.05 to 0.05 electron/Å^3 in first row and from -0.03 to 0.03 electron/Å^3 in second row. The electron deficiency is marked in blue, and the electron enrichment in red. The additional Cu-Ti bonding around the Cu substitutions are found in Fig. 3(c) and Fig. 3(e). Blue-spheres liked electrons deficiencies areas locate around the Cu-substitutions. Moreover, two large and one small irregular electron enrichments areas seat near these blue-spheres, as the white dash-circles and dot-circles shown in Fig. 3(d) and Fig. 3(f), respectively. In Fig. 3(i) and Fig. 3(k), the additional Cu-O bonds are found as shown by the white-arrows. Three blue-spheres liked electrons deficiencies areas locate around the Cu-substitutions. Three blocks of irregular electron enrichments seat near the three blue spheres in Figs. 3(j) and 3(l). Obviously, the more electrons-holes recombination leads to the less electrons enrichment as the white dot-circles shown in Fig. 3(d) and Fig. 3(f); while the larger electrons aggregations exist as the three white-circles shown Fig. 3(j) and Fig. 3(l). Accordingly, the larger dipoles around Cu-ions would result in the larger internal electric fields and weaken the recombination of electrons-holes.

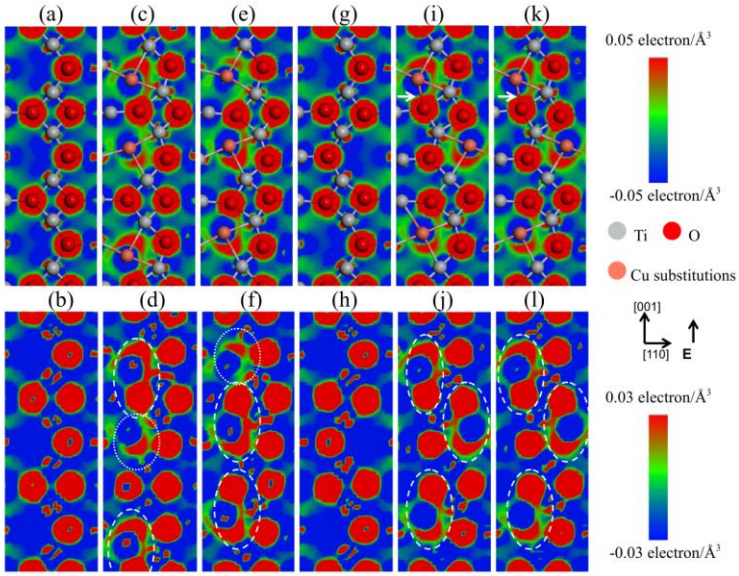

Fig. 3 Partial sectional view at [110] facet and the corresponding deformation electron density for VOSA under 1.3 MV/cm (a, b), CuSA under 1.3 MV/cm (c, d) and 10.4 MV/cm (e, f), VODF under 1.3 MV/cm (g, h), CuDF under 1.3 MV/cm (i, j) and 10.4 MV/cm (k, l).

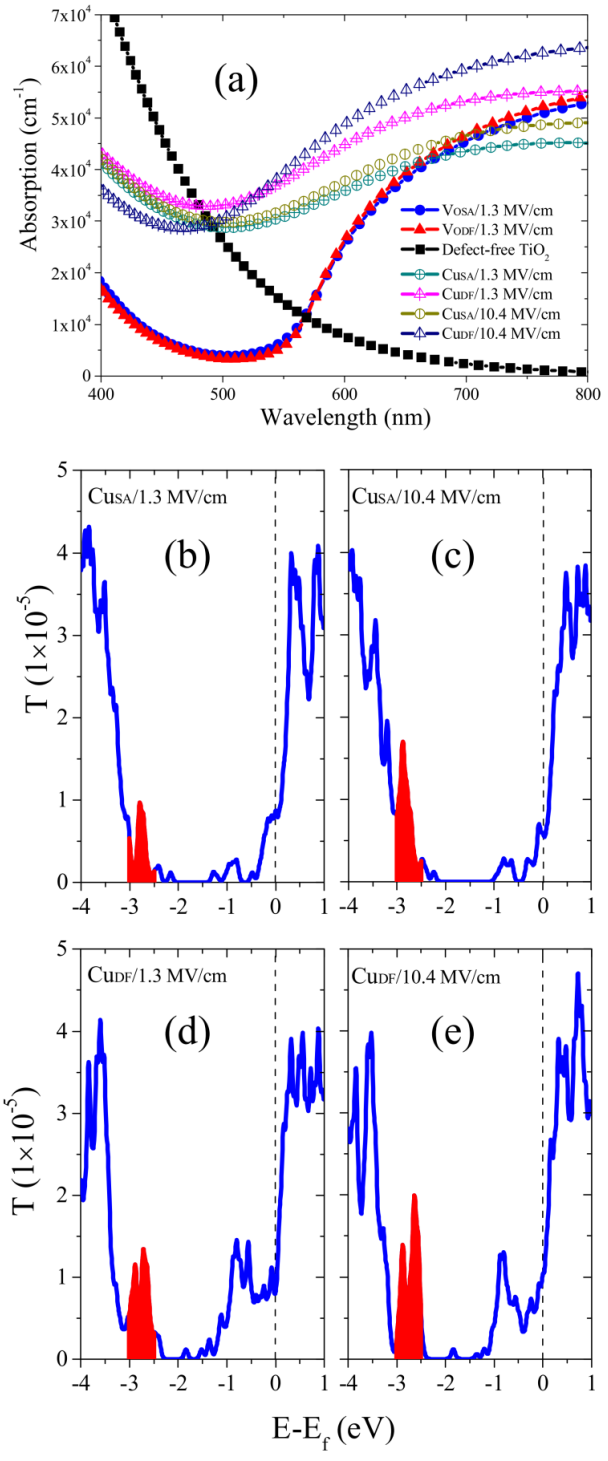

Fig. 4. (a) Visible light absorption spectra of the defect-free TiO_2, VOSA and VODF, CuSA and CuDF under 1.3 MV/cm and 10.4 MV/cm; Transmission coefficients in CuSA under 1.3 MV/cm (b) and 10.4 MV/cm (c), CuDF under 1.3 MV/cm (d) and 10.4 MV/cm (e).

Fig. 4(a) shows the visible light absorption spectra of the defect-free TiO_2, *VOSA* and *VODF*, *CuSA* and *CuDF* under 1.3 MV/cm and 10.4 MV/cm. In Fig. 4(a), *CuSA* and *CuDF* exhibit relatively larger absorption than that in defect-free TiO_2 at 490–800 nm. As a comparison, the visible light absorptions in *CuDF* are larger than those in *CuSA*. It originates from the formation of the more dipoles in *CuDF* as shown in Fig. 3. The relaxed structures under the higher electric field (10.4 MV/cm) lead to the higher absorption than those under the lower electric field (1.3 MV/cm). At 700–800 nm, the absorptions in *VOSA* and *VODF* under the higher electric field (10.4 MV/cm) are larger than those in *CuSA*, while still smaller than those in *CuDF*. It illustrates that only the Cu-substitutions in the different-sides more efficiently improve the absorption of visible light. The transmission coefficient could also verify the above conclusions, as shown in Fig. 4(b–e). In Fig. 4(c) and Fig. 4(e), the transmission coefficients at -3 eV ~ -2.5 eV are larger than those in Fig. 4(b) and Fig. 4(d). Moreover, the transmission coefficients at -1 eV ~ -0.5 eV in Fig. 4(d) and Fig. 4(e) are also larger than those in Fig. 4(b) and Fig. 4(c). It illustrates the less recombination of electrons and holes and the more delocalized electrons in *CuDF* under higher electric field.

4. Conclusions

We have performed *ab initio* calculations to study the visible light absorption at different locations of the Cu-substitutions and the electric fields in the defective TiO_2. It demonstrates that these Cu-substitutions on different sides around central Ti-ions strengthened visible light absorption rather than those on same sides do. This is attributed to that the production of the more dipoles between the Cu-ions and the O-ions in former structures weakens the recombination of electrons and holes, especially under higher electric fields. This also delocalizes the electrons which should be attracted by the adjacent O-ions. Consequently, the Cu-substitutions and applied electric field together determine the characteristics of the visible-light absorption of defective TiO_2.

Acknowledgments

The authors acknowledge the support from the National Natural Science Foundation of China under grant Nos. 61774014, and 61272105, Natural Science Foundation of Jiangsu Province of China under grant No. BK20141196. We also would like to thank the editors and reviewers for their time spent on conducting our manuscript and their comments helping us improving the article.

References

[1] G. Gustafsson, Y. Cao, G. M. Treacy, F. Klavetter, N. Colaneri, A. J. Heeger, Nature **357**(6378), 477 (1992).

[2] D. C. Look, K. D. Leedy, D. H. Tomich, B. Bayraktaroglu, Applied Physics Letters **96**(6), 062102 (2010).
[3] K. L. Chopra, S. K. Major, D. K. Pandya, Thin Solid Films **102**(1), 1 (1983).
[4] A. Dhar, T. L. Alford, Journal of Applied Physics **112(**10), 103113 (2012).
[5] C. Guillen, J. Herrero, Thin Solid Films **520**(1), 1 (2011).
[6] K. Sivaramakrishnan, N. D. Theodore, J. F. Moulder, T. L. Alford, Journal of Applied Physics **106(**6), 063510 (2009).
[7] A. Fujishima, K. Honda, Nature **238(**5385), 37 (1972).
[8] S. A. Ansari, M. H. Cho, Scientific Reports **6**, 25405 (2016).
[9] S. Na-Phattalung, M. F. Smith, K. Kim, M. H. Du, S. H. Wei, S. B. Zhang, S. Limpijumnong, Physical Review B **73(**12), 125205 (2006).
[10] B. J. Morgan, G. W. Watson, Journal of Physical Chemistry C **113(**17), 7322 (2009).
[11] X. Cui, B. Wang, Z. Wang, T. Huang, Y. Zhao, J. Yang, J. G. Hou, Journal of Chemical Physics **129**(4), 044703, (2008).
[12] C. M. Yim, C. L. Pang and G. Thornton, Physical Review Letters, **104**(3), 036806 (2010).
[13] H. Tang, K. Prasad, R. Sanjines, P. E. Schmid, F. Levy, Journal of Applied Physics **75**(4), 2042 (1994).
[14] J. J. Yang, M. D. Pickett, X. Li, D. A. Ohlberg, D. R. Stewart, R. S. Williams, Nature Nanotechnology **3**(7), 429 (2008).
[15] J. Choi, H. Park, M. R. Hoffmann, Journal of Physical Chemistry C **114(**2), 783 (2009).
[16] W. Guan, M. Liu, S. Long, Q. Liu, W. Wang, Applied Physics Letters **93(**22), 223506 (2008).
[17] Q. Liu, S. Long, W. Wang, Q. Zuo, S. Zhang, J. Chen, M. Liu, IEEE Electron Device Letters **30**(12), 1335 (2009).
[18] M. Gratzel, R. F. Howe, Journal of Physical Chemistry **94**(6), 2566 (1990).
[19] E. C. Butler, A. P. Davis, Journal of Photochemistry and Photobiology A: Chemistry **70**(3), 273 (1993).
[20] W. Choi, A.Termin, M. R. Hoffmann, Journal of Physical Chemistry **98(**51), 13669 (1994).
[21] M. Janousch, G. I. Meijer, U. Staub, B. Delley, S. F. Karg, B. P. Andreasson, Advanced Materials **19(**17), 2232 (2007).
[22] H. Y. Kim, H. M. Lee, G. Henkelman, Journal of the American Chemical Society **134**(3), 1560 (2012).
[23] J. G. Chang, H. T. Chen, S. P. Ju, H. L. Chen, C. C. Hwang, Langmuir **26**(7), 4813 (2010).
[24] L. Li, W. Li, A. Ji, Z. Wang, C. Zhu, L. Zhang, J. Yang, L. F. Mao, Physical Chemistry Chemical Physics **17(**27), 17880 (2015).
[25] J. P. Perdew, K. Burke, M. Ernzerhof, Physical Review Letters **77**(18), 3865 (1996).
[26] H. J. Monkhorst, J. D. Pack, Physical Review B **13(**12), 5188 (1976).
[27] M. D. Segall, P. J. D. Lindan, M. J. Probert, C. J. Pickard, P. J. Hasnip, S. J. Clark, M. C. Payne, Journal of Physics: Condensed Matter **14**(11), 2717 (2002).
[28] Atomistix Tool Kit version 2015.0, Quantum Wise A/S.
[29] M. Brandbyge, J.-L. Mozos, P. Ordejón, J. Taylor, K. Stokbro, Physical Review B **65**, 165401 (2002).

*Corresponding author: mail_lingfeng@aliyun.com; lei_li56@163.com